ELSEVIER

Physics of the Earth and Planetary Interiors 106 (1998) 257–273

PHYSICS OF THE EARTH AND PLANETARY INTERIORS

Anisotropic tomography of the Atlantic Ocean from Rayleigh surface waves

Graça Silveira [a,b,c,*], Eléonore Stutzmann [d], Daphné-Anne Griot [d], Jean-Paul Montagner [d], Luis Mendes Victor [a,b]

[a] *Centro de Geofísica da Universidade de Lisboa, Rua da Escola Politécnica, 58, P-1250 Lisboa, Portugal*
[b] *Departamento de Física da Faculdade de Ciências, Universidade de Lisboa, Edifício C1, Campo Grande, P-1700 Lisboa, Portugal*
[c] *Instituto Superior de Engenharia de Lisboa, Rua Conselheiro Emídio Navarro, P-1800 Lisboa, Portugal*
[d] *Département de Sismologie, Institut de Physique du Globe 4, place Jussieu, 75252 Paris Cedex 05, France*

Received 30 June 1997; accepted 24 December 1997

Abstract

The depth extent of the Mid Atlantic Ridge and the role of hotspots in the Atlantic opening are still a matter of debate. In order to constrain the structure and the geodynamic processes below the Atlantic Ocean, we provide the first anisotropic phase velocity maps of this area, obtained at a regional scale. We have determined Rayleigh wave phase velocities along 1311 direct epicentre to station paths. For each path, phase velocities are calculated by a technique of cross-correlation with a synthetic seismogram. These phase velocities are corrected for the effect of shallow layers. They are then inverted, without a priori constraints, to obtain maps of the lateral variations of the anisotropic phase velocities in the period range 50–250 s. The ridge axis corresponds to a low velocity anomaly, mainly visible at short periods. A good correlation between hotspot locations and low velocity anomalies is obtained for the whole period range. Furthermore, a low velocity anomaly elongated along a North–South direction is visible for every period and seems to be correlated with hotspot positions. On average, the North Atlantic is associated with higher velocities than the South Atlantic. The shields below Canada, Brazil and Africa display high velocity anomaly at short periods and only the Brazilian and African shields are still visible for a period of 200 s, thus suggesting that the Canadian shield is a shallower structure. The maps of phase velocity anisotropy under the Atlantic Ocean are interpreted in the Mid-Atlantic area, where we have the best resolution. Close to the ridge, the fast axis of Rayleigh wave phase velocity is found perpendicular to the ridge axis. A comparison of anisotropy directions and plate motion shows that seismic anisotropy integrates also deeper phenomena such as mantle convection.

Keywords: Anisotropic tomography; Atlantic ocean; Rayleigh surface waves; Mid Atlantic ridge

1. Introduction

The last re-opening of the Atlantic Ocean dates from about 180 Ma. With the exception of the Antilles and Sandwich islands, it is surrounded by passive margins. Its most prominent feature is the Mid Atlantic Ridge (MAR) which is found to be a shallow structure, visible only down to about 250 km depth on tomographic models (Montagner and Tanimoto, 1990, 1991). It has a low spreading rate

* Corresponding author.

0031-9201/98/$19.00
PII S0031-9201(98)00079-X

ranging from 1 to 4 cm/year and its origin at depth is not well established. Due to this low spreading rate, the age of the ocean floor rapidly increases with the distance from the ridge axis. The ridge axis has a North–South direction in the South Atlantic and deviates to the West in the North Atlantic. A striking feature is the alignment of hotspots along a roughly North–South direction in the whole Atlantic. They are located along the ridge axis in the South Atlantic but off the ridge axis in the North Atlantic. A better knowledge of their lateral and depth extent will enable us to understand their origin and their role in mantle convection.

During the last two decades, the development of broadband seismograph global networks, combined with the improvement of computers have enabled scientists to produce tomographic models of the Earth with increasing resolution. The first generation of models have only used the travel time or phase of seismograms to provide isotropic models. Later, parameterization of the anisotropy and anelasticity was included in the models (among others: Montagner, 1986b; Montagner and Jobert, 1988; Bussy et al., 1993; Griot, 1997). More recently, geodynamic constraints have been taken into account (as in Forte et al., 1994), and other models have been derived from waveform inversion (among others; Stutzmann and Montagner, 1994; Li and Romanowicz, 1996; Debayle and Lévêque, 1997). These models provide a three dimensional image of the Earths mantle at a global scale as well as at a regional scale.

When comparing regions of similar ages, the amplitude of velocity anomalies is always higher under the Atlantic Ocean than under the Pacific Ocean (among others: Montagner and Tanimoto, 1991; Ekström et al., 1997). The ridge axis is the only striking feature when we zoom in on the Atlantic on global tomographic models. Recently, Trampert and Woodhouse (1995, 1996) have obtained an almost continuous low phase velocity anomaly under the MAR for Love waves of periods larger than 79 s. This low velocity anomaly, however, is not so visible on their Rayleigh wave phase velocity maps, even at short periods. In contrast, the global Rayleigh wave phase velocity maps of Ekström et al. (1997) display a nearly continuous low velocity anomaly along the Mid-Atlantic Ridge for periods ranging from 50 to 150 s. On the other hand, the Zhang and Lay (1996) phase velocity maps provide velocity anomalies that are not well correlated with the ridge axis.

Global tomographic models mainly enable us to distinguish the MAR and the oceanic basins. Small scale features under the Atlantic Ocean can only come out from regional studies. Unfortunately, the Atlantic Ocean is not very suitable for regional tomographic studies due to the lack of seismicity. Indeed, Mid-Atlantic ridge presents low seismic activity and there is little seismicity around the Ocean. Weidner (1974) was the first to correlate regional lateral variations of surface wave phase velocities with different sediment thicknesses between ridges and basins. Later, Canas and Mitchell (1981) related shear wave velocity anomalies to the age of the Atlantic Ocean floor. Honda and Tanimoto (1987) performed waveform inversion to obtain the first regional three dimensional model of the Atlantic Ocean. At shallow depths, they obtained low velocities beneath the Azores triple junction and under Europe and high velocities beneath the Canadian shield and in the Central Atlantic. Mocquet et al. (1989) confirm the existence of a high phase velocity anomaly (for periods larger than 100 s) beneath the Central Atlantic. Later, Mocquet and Romanowicz (1990), using surface wave phase velocities, and Grand (1994), using S-wave travel times, presented new Atlantic regional three dimensional models. We can summarize robust features of all these models as follows: (1) the North Atlantic lithosphere is characterized by slower velocities beneath the MAR than under the old ocean basins; (2) the Atlantic asthenosphere structure does not exhibit deep low velocity anomalies below the MAR and, furthermore, the central part of the ridge displays a high velocity anomaly for depths greater than 300 km.

The mapping of seismic velocity anomalies is getting progressively consistent between different studies, but azimuthal anisotropy patterns are still a matter of debate. Kuo et al. (1987) explain their SS–S differential travel times in the North Atlantic by azimuthal anisotropy which is compatible with a mantle flow in a North–South direction. This model however is incompatible with results obtained by Sheehan and Solomon (1991) by a combined inversion of SS–S differential travel times, geoid height and bathymetric depth anomaly. Yang and Fischer (1994) explain the discrepancy between these two

studies by taking into account the variation of SSV/SSH amplitude ratio. On the other hand, Kuo and Forsyth (1992) study SKS splitting and find anisotropy amplitudes smaller than in previous studies.

In order to improve lateral resolution of velocity models under the Atlantic Ocean and to provide the first maps of anisotropy directions on a regional scale, we have performed a tomographic study of this area using Rayleigh wave phase velocities. Phase velocities are calculated by a technique of cross-correlation with a synthetic seismogram for each path. These phase velocities are then corrected to take into account the effect of shallow layers. In a second step, they are inverted, without a priori constraints, to obtain phase velocity lateral variations and anisotropy in the period range 50–250 s. The results are then discussed in the framework of mantle convection and evolution of the Atlantic Ocean.

2. Method

2.1. Phase velocity measurement

For each epicentre-to-station path, phase velocity is computed by cross-correlating the data with a synthetic seismogram. The synthetic seismogram is computed by normal mode summation for a given reference Earth model, source parameters and instrumental response (Woodhouse and Girnius, 1982). The phase difference, $\phi - \phi_o$, between observed and synthetic seismograms gives the delay time τ between the two signals as a function of angular frequency ω:

$$\delta\tau(\omega) = \frac{\phi(\omega) - \phi_o(\omega)}{\omega} \quad (1)$$

Then phase velocity V is computed using the following relation:

$$\frac{\Delta}{V(\omega)} = \frac{\Delta}{V_o(\omega)} + \delta\tau \quad (2)$$

where Δ is the epicentral distance and V_o the reference phase velocity.

2.2. Phase velocity error estimation

Errors on phase velocity determination for a given epicentre-to-station path are mainly due to seismic source uncertainties and instrument approximations. Errors due to instrumental response can be neglected because new broadband instruments are well calibrated. We take into account errors due to the sampling rate, that is $\delta t_1 = 10$ s. Only the direct paths between epicentre and station are used and, therefore, the effect of lateral refraction can be neglected. Seismic source uncertainties can be estimated from nuclear explosions. Mislocations of nuclear explosions give an upper limit of 20 km for the uncertainty on epicentral locations. Error on earthquake origin time is considered here together with error on source time function, with $\delta t_2 = 5$ s.

Different estimations of errors δt_i are assumed to be independent and Gaussian. The error estimation on slowness can be computed as follows:

$$\delta(1/V) = \frac{1}{\Delta}\delta t = \frac{1}{\Delta}\left[\delta t_1^2 + \delta t_2^2 + \left[\frac{\mathrm{d}\Delta}{V}\right]^2\right]^{1/2} \quad (3)$$

where V is the phase velocity and Δ the epicentral distance.

2.3. Regionalization

The fundamental mode phase velocity is computed for every path. In a second step, these phase velocities are inverted to obtain, for each period, a map of phase velocity lateral variations and anisotropy. Using Rayleigh's principle combined with harmonic tensor decomposition of Backus (1970), Smith and Dahlen (1973) have shown that for a slight anisotropic earth, the local phase velocity at a given

point M, can be expressed, for each angular frequency ω, by:

$$V(\omega,M,\psi) = V_o(\omega,M)\left[1 + \alpha_1(\omega,M)\cos(2\psi) + \alpha_2(\omega,M)\sin(2\psi) + \alpha_3(\omega,M) \times \cos(4\psi) + \alpha_4(\omega,M)\sin(4\psi)\right] \quad (4)$$

where ψ is the azimuth of the considered direction and α_i the coefficients of azimuthal anisotropy. Montagner and Nataf (1986) have shown that Rayleigh waves are mainly sensitive to 2 ψ-coefficients. Therefore in the following, we have only inverted phase velocity for isotropic velocity given by V_o and the 2 anisotropic coefficients α_1, α_2.

The relation between average phase velocity for a given path from the epicentre E to the station S, $V(\omega,\psi)$ and local phase velocity at a position M can be written:

$$\frac{\Delta}{V(\omega,\psi)} = \int_E^S \frac{ds}{V_o(\omega,M)} - \int_E^S \frac{ds}{V_o(\omega,M)} \times \left[\alpha_1(\omega,M)\cos(2\psi) + \alpha_2(\omega,M)\sin(2\psi)\right] \quad (5)$$

Following Montagner (1986a), the under-determined problem is solved by using a continuous formulation of the inverse problem proposed by Tarantola and Valette (1982). Parameter $\boldsymbol{p}$ is a vector composed of three independent distributions V_o, α_1 and α_2. The data, $\boldsymbol{d}$, is the vector of measured phase velocities for all paths. The reference model slowness is noted $\boldsymbol{p}_o$ and we have:

$$\boldsymbol{p}(\boldsymbol{r}) - \boldsymbol{p}_o(\boldsymbol{r}) = \sum_{i=1}^{n_d}\sum_{j=1}^{n_d}\int_{path_i} C_{p_o}(\boldsymbol{r},\boldsymbol{r_i}) G_i^T \frac{ds_i}{\Delta_i} S_{ij}^{-1} \times \left\{ \boldsymbol{d}_j - \int_{path_j} G_j \boldsymbol{p}_o(\boldsymbol{r_j}) \frac{ds_j}{\Delta_j} \right\} \quad (6)$$

with

$$S_{ij} = C_{d_{ij}} + \int_{path_i} G_i \frac{ds_i}{\Delta_i} \int_{path_j} C_{p_o}(\boldsymbol{r_i},\boldsymbol{r_j}) G_j^T \frac{ds_j}{\Delta_j}$$

where G is the Frechet derivative matrix of Eq. (5); $C_{\boldsymbol{d}}$ is the covariance matrix of the data. The matrix is diagonal and corresponds to the square of the errors on slowness computed for each path (using relation 3); $C_{\mathbf{p}_o}$ is the a priori covariance function on the parameters. In order to regularize the inversion, it is necessary to introduce a correlation length, L_{corr}, which depends on the path coverage of the Earth. This covariance function between 2 points $\boldsymbol{r}_1$ and $\boldsymbol{r}_2$ is defined by:

$$C_{p_o}(\boldsymbol{r_1},\boldsymbol{r_2}) = \sigma(\boldsymbol{r_1})\sigma(\boldsymbol{r_2})\exp\left[\frac{\cos\Delta_{\mathbf{r}_1\mathbf{r}_2} - 1}{L_{cor}^2}\right] \quad (7)$$

where σ is the a priori error on the parameters at the location $\boldsymbol{r}$ and Δ is the epicentral distance.

The a posteriori error on the model is defined by the square root of the diagonal term of the a posteriori covariance matrix (Tarantola and Valette, 1982):

$$C_{post}(\boldsymbol{r_1},\boldsymbol{r_2}) = C_{p_o}(\boldsymbol{r_1},\boldsymbol{r_2}) - \sum_{i=1}^{n_d}\sum_{j=1}^{n_d}\int_{path_i} C_{p_o}(\boldsymbol{r_1},\boldsymbol{r_2})\frac{ds_i}{\Delta_i} \times \int_{path_j} G_i (S^{-1})_{ij} G_j^T C_{p_o}(\boldsymbol{r_1},\boldsymbol{r_2})\frac{ds_j}{\Delta_j} \quad (8)$$

3. Data

3.1. Data selection

We have selected events occurring at the Mid-Atlantic Ridge and all around the Atlantic Ocean, with a magnitude larger than 5.8 and a known centroid moment tensor (CMT). Unfortunately, the MAR and Atlantic coast seismicity is characterized mostly by earthquakes of magnitude smaller than 5.8 for which no CMT is computed and corresponding to signal with a high noise level. Furthermore, there is an evident lack of broadband or long period digital seismic stations in and around the Atlantic Ocean. Therefore, we have also used events from the west South American coast, the Mediterranean region and Central Africa. We have selected 10 GEOSCOPE

and 25 IRIS seismic stations that are located close to the Atlantic area and were operational between 1987 and 1994. We have used both vertical and longitudinal components of the VLP (Very Long Period) channel (0.1 Hz). The geographical distribution of the 1311 paths used in this study is presented in Fig. 1.

An example of the data and synthetic seismogram for the vertical component recorded at the ECH seismic station, for the Peru earthquake of 15 April 1991, is shown in Fig. 2a. The corresponding phase velocity is plotted in Fig. 2b. We have considered the PREM model as a reference model (Dziewonski and Anderson, 1981).

3.2. Tests on inversion reliability

Phase velocities have been inverted to obtain lateral variations and anisotropy, in the period range 50–250 s.

We have performed the inversion for different windows of the study area in order to check that the peripheral areas do not affect the seismic velocity distribution in the best resolved area, that being the central Atlantic. Results are presented for latitudes between 40°S and 60°N and for longitudes between 100°W and 20°E.

Inversion results are controlled by two parameters, the a priori error on parameters and the correla-

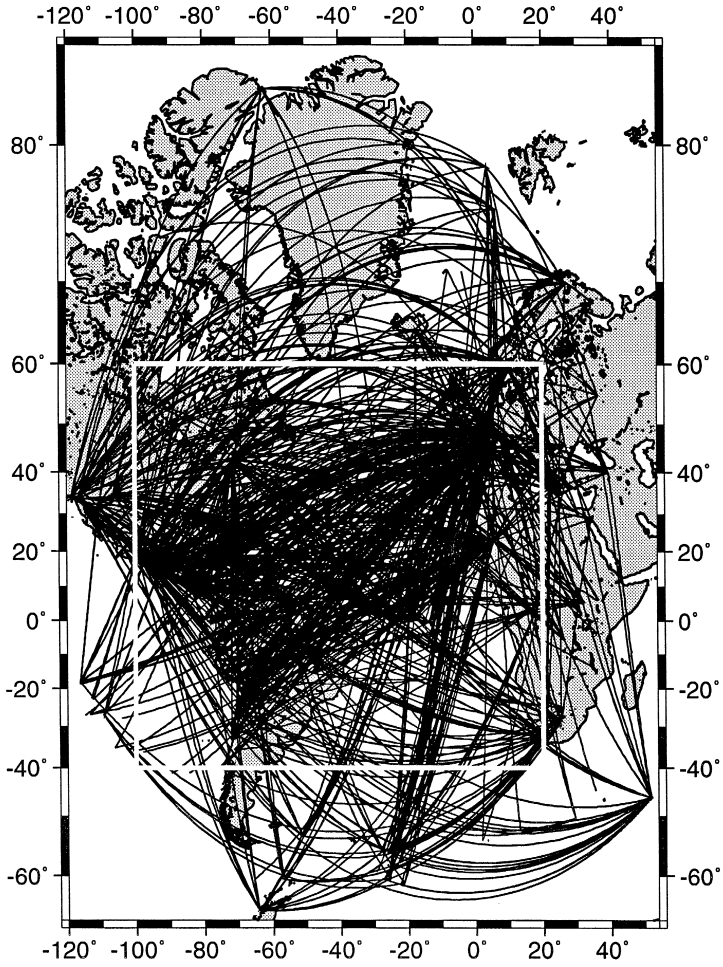

Fig. 1. Geographical distribution of the 1311 paths used in this study.

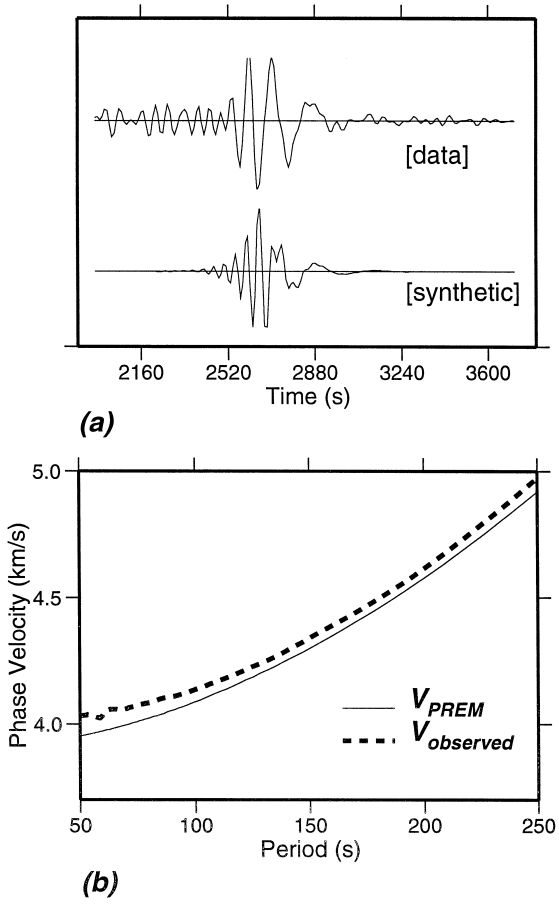

Fig. 2. Vertical seismogram recorded by station ECH (Echery) of the Peru earthquake of 5 April 1991. (a) Comparison of observed and synthetic seismograms. (b) Phase velocities as a function of period. Dashed line and continuous line correspond respectively to the observed and model phase velocities.

tion length. The a priori error on parameters corresponds to uncertainties on velocities and anisotropy, and defines the variation range of the model parameters. The correlation length L_{corr} is directly related to the wavelength of the final model anomalies. In a first approximation, it can be estimated from the surface of the studied area, S, the number of data, n_d, and the number of inverted parameters, n_p, with the relation (Stutzmann and Montagner, 1994):

$$L_{\mathrm{corr}}^2 = \frac{S n_p}{n_d} \tag{9}$$

We obtain $L_{\mathrm{corr}} \simeq 5.2^\circ \simeq 580$ km.

To check the reliability of the inversion, we have performed several inversions for different correlation lengths, L_{corr}, and the a priori error on velocities, σ_{vel}, and on anisotropy, σ_{ani}. For each inversion, we have computed: (a) the a posteriori error on velocities defined by Eq. (8); (b) the data misfit:

$$S(\boldsymbol{p}) = \sqrt{\frac{1}{n_d}\sum_{i=1}^{n_d}\left[\boldsymbol{d}_i - g_i(\boldsymbol{p})\right]^2} \tag{10}$$

where n_d is the number of data; and (c) the amplitude of the heterogeneities defined by

$$A = \left[\frac{\int_\theta\int_\varphi \left(V_R(\theta,\varphi) - V_{\mathrm{o}}\right)^2 \sin\theta \,\mathrm{d}\theta \,\mathrm{d}\varphi}{\int_\theta\int_\varphi \sin\theta \,\mathrm{d}\theta \,\mathrm{d}\varphi}\right]^{1/2} \tag{11}$$

where $V_R(\theta,\varphi)$ is the local phase velocity after inversion in a point of coordinates (θ,φ), V_{o} is the mean phase velocity, and (θ,φ) are, respectively, the latitude and longitude.

These three functions are presented as a function of correlation length in Fig. 3, of velocity a priori error in Fig. 4 and of anisotropy a priori error in Fig. 5. The inverse problem is well resolved when the a posteriori error is smaller than the a priori error. The a posteriori error and the data misfit have to be as small as possible. Finally, the amplitude of heteregeneities shows how phase velocity maps are perturbed by the inversion parameters (correlation length and a priori errors).

A good compromise between resolution and a posteriori errors corresponds to a correlation length of 750 km (Fig. 3a and b). Moreover, this correlation length provides the largest amplitudes of the model heterogeneities.

Fig. 4a shows that the a posteriori error on velocities depends linearly on the velocity a priori error. The amplitude of heteregeneities also increases with a priori error (Fig. 4c). On the other hand, the data misfit is not affected by this parameter in the range of 0.1–0.3 km/s. This illustrates the difficulty of resolving the absolute amplitude of velocities in tomographic studies. We have therefore selected an intermediate value of 0.2 km/s.

Fig. 5a shows that the velocity a posteriori errors also depends linearly on the anisotropy a priori errors. The data misfit decreases when anisotropy is

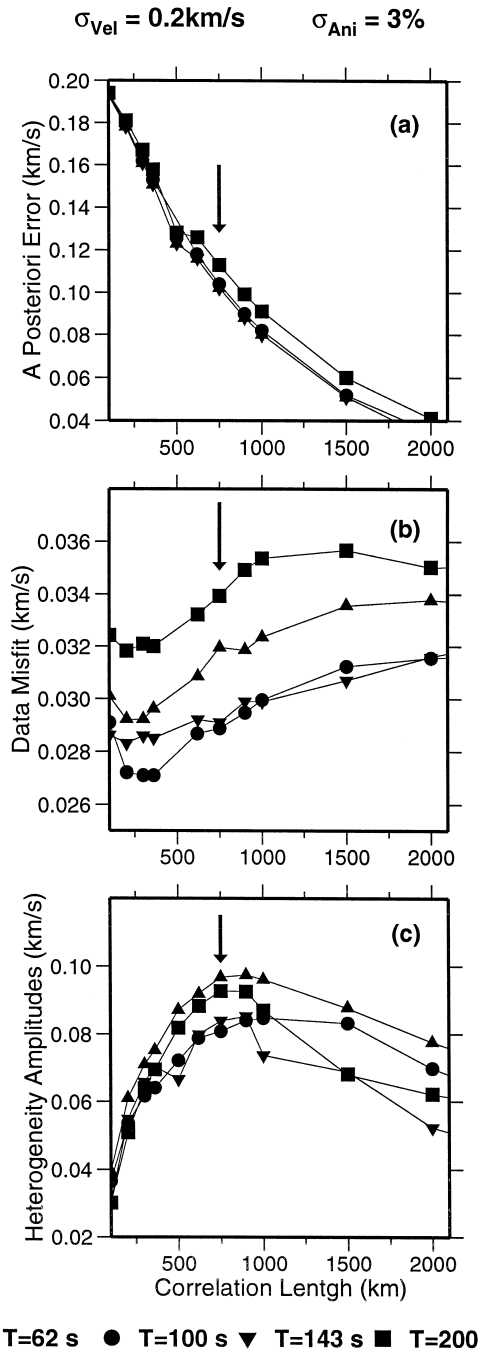

Fig. 3. Variation of the a posteriori error (a), the data misfit (b) and the amplitude of the heterogeneities (c) as a function of the correlation length.

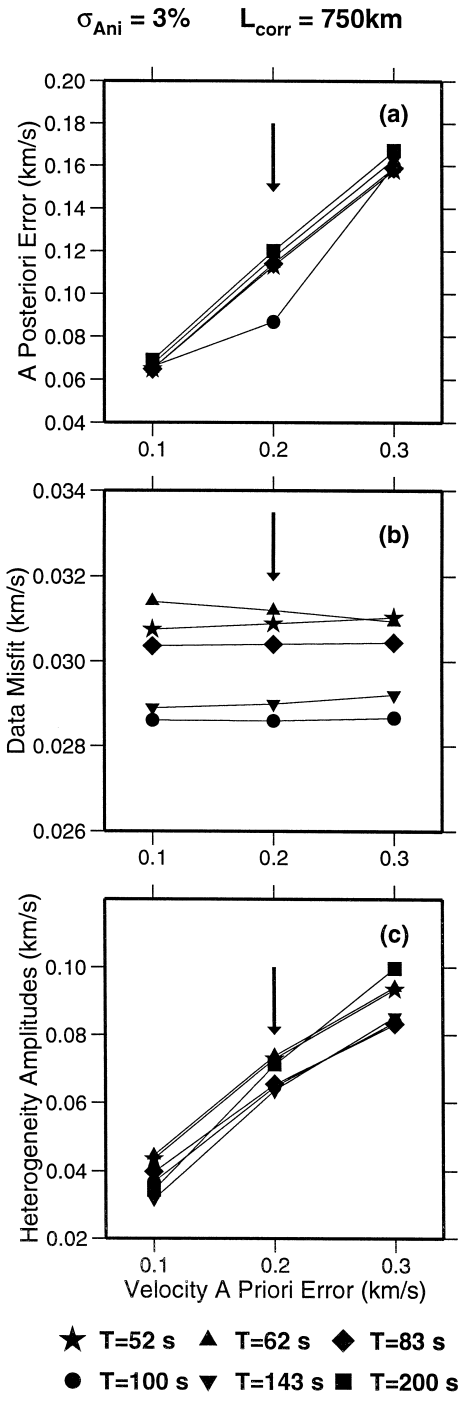

Fig. 4. Variation of the a posteriori error (a), the data misfit (b) and the amplitude of the heterogeneities (c) as a function of the a priori error on velocities.

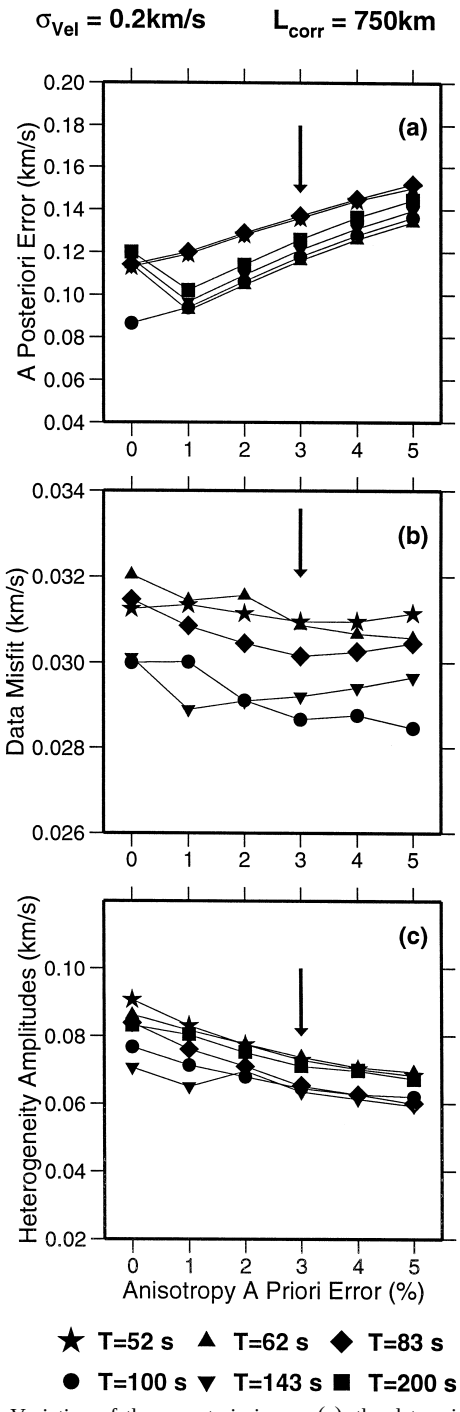

Fig. 5. Variation of the a posteriori error (a), the data misfit (b) and the amplitude of the heterogeneities (c) as a function of the a priori error on anisotropy (in percentage).

taken into account (Fig. 5b) and is at a minimum for a percentage of anisotropy of 3%. The isotropic part of the amplitude of the model heterogeneities decreases in the anisotropic models (Fig. 5c). Fig. 6 confirms the need to take into account the anisotropy in the inversion. It shows that the variance reduction is better when 3–4% of the a priori error on anisotropy is considered. Furthermore, anisotropy almost does not change the location of the isotropic component of velocities but modify slightly its amplitude, as can be seen in Fig. 7. Table 1 summarizes parameters used in the inversion. Finally, we have checked that the inversion results are not biased by a preferential orientation of some paths in the NW–SE direction. We have performed the same inversion with a sub-dataset consisting of a more homogeneous azimuthal path coverage and we have obtained similar results as with the entire dataset.

3.3. Shallow layer corrections

Variations of shallow layers (bathymetry, topography and crustal thickness) are important between ocean and continent and even under the ocean, they

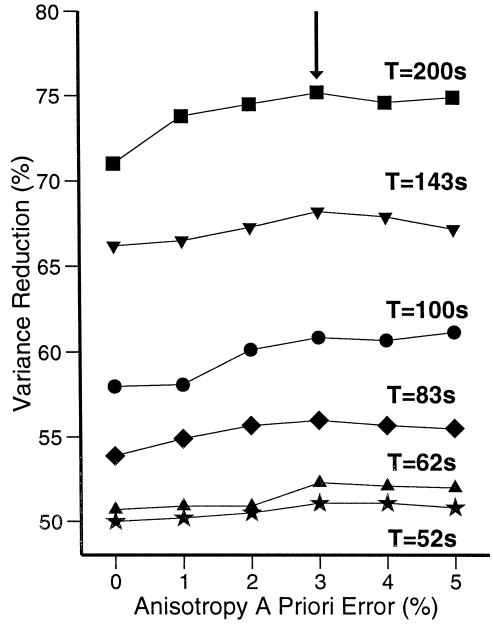

Fig. 6. Variance reduction as a function of a priori error on anisotropy.

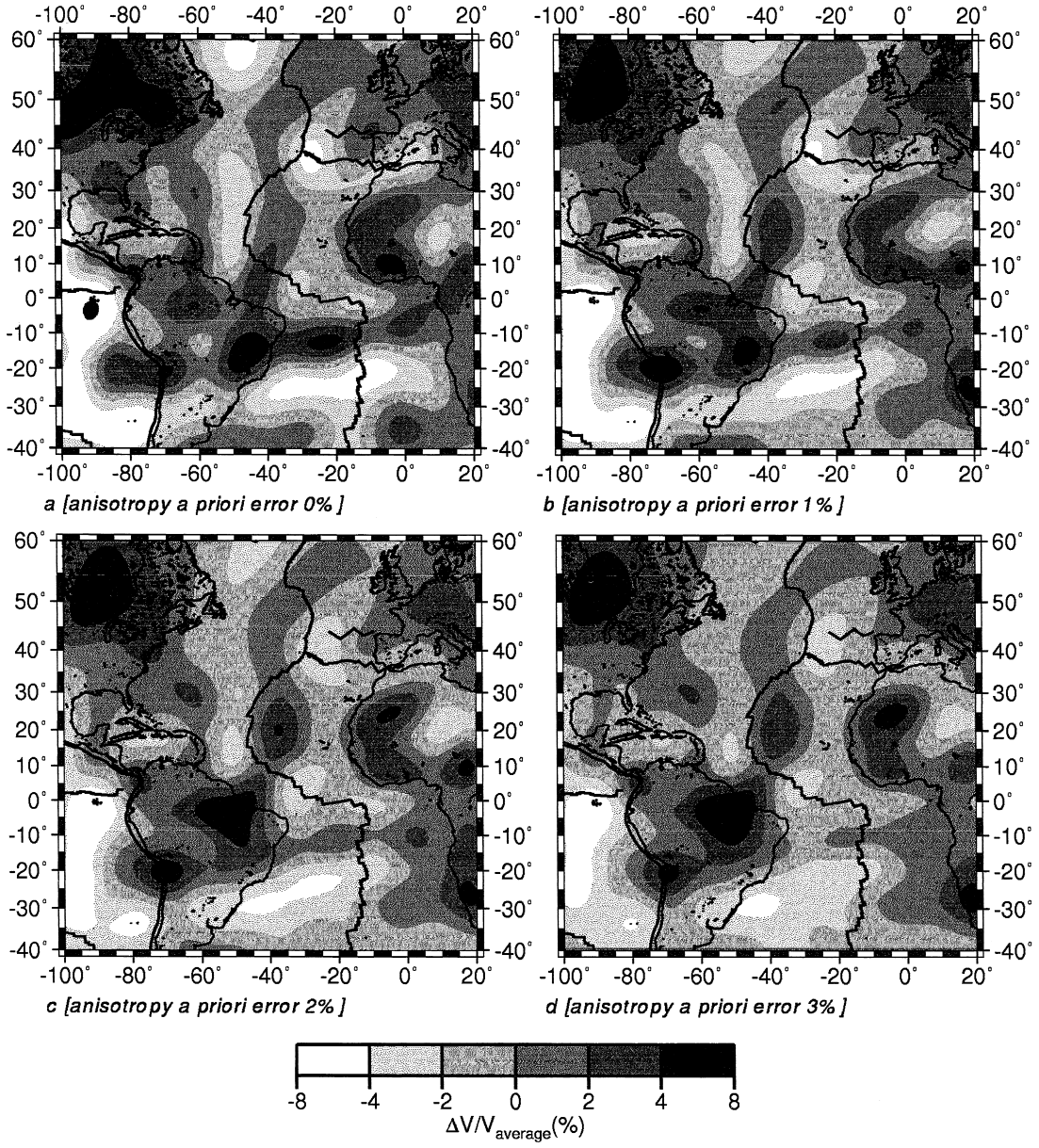

Fig. 7. Phase velocity perturbation maps obtained for a period of 100 s. They are computed with respect to the map average velocity and expressed in percent. (a) Isotropic inversion (b–c–d) Anisotropic inversion with an a priori error on anisotropy of 1%, 2% and 3%, respectively.

vary as a function of sea floor age. Stutzmann and Montagner (1994), among others, have shown that the influence of Moho depth on fundamental mode surface waves is very important at short periods and decreases with increasing periods. The frequency content of the data is dominantly long period and therefore cannot resolve shallow structures. A poor account of these structures, however, can bias the

Table 1
Parameters used in the inversion. σ_{data}: data error; L_{corr}: correlation length; $\sigma_{velocity}$: a priori error on velocity; $\sigma_{anisotropy}$: a priori error on anisotropy

σ_{data}	0.02–0.08 km/s (see Eq. (3))
L_{corr}	750 km
$\sigma_{velocity}$	0.2 km/s
$\sigma_{anisotropy}$	3%

deep structures. Therefore, the data have been corrected for crustal effect. Phase velocity crustal perturbations have been computed for model 3SMAC (Nataf and Ricard, 1996) and subtracted from our data. The phase velocities have been corrected path by path before inversion. As shown in Fig. 8, for a period of 62 s, the effect of shallow layer correction increases the amplitude of velocity anomalies but does not change their location. Moreover, shallow layer correction does not change anisotropy amplitude and direction.

4. Results and discussion

4.1. Phase velocity distribution

Data corrected from the effect of shallow layers have been inverted using the a priori parameters presented in Table 1. Maps of the isotropic component of phase velocity, (coefficient V_o in Eq. (4)), are presented in Fig. 9 for several periods: 57, 100, 167 and 200 s. In a first approximation, the period can be converted into the maximum depth sensitivity D using the relation $D = TV/3$, where T is the period and V is the phase velocity. The a posteriori error maps are presented in Fig. 10 for the same periods. At short periods (Fig. 9a) the phase velocity

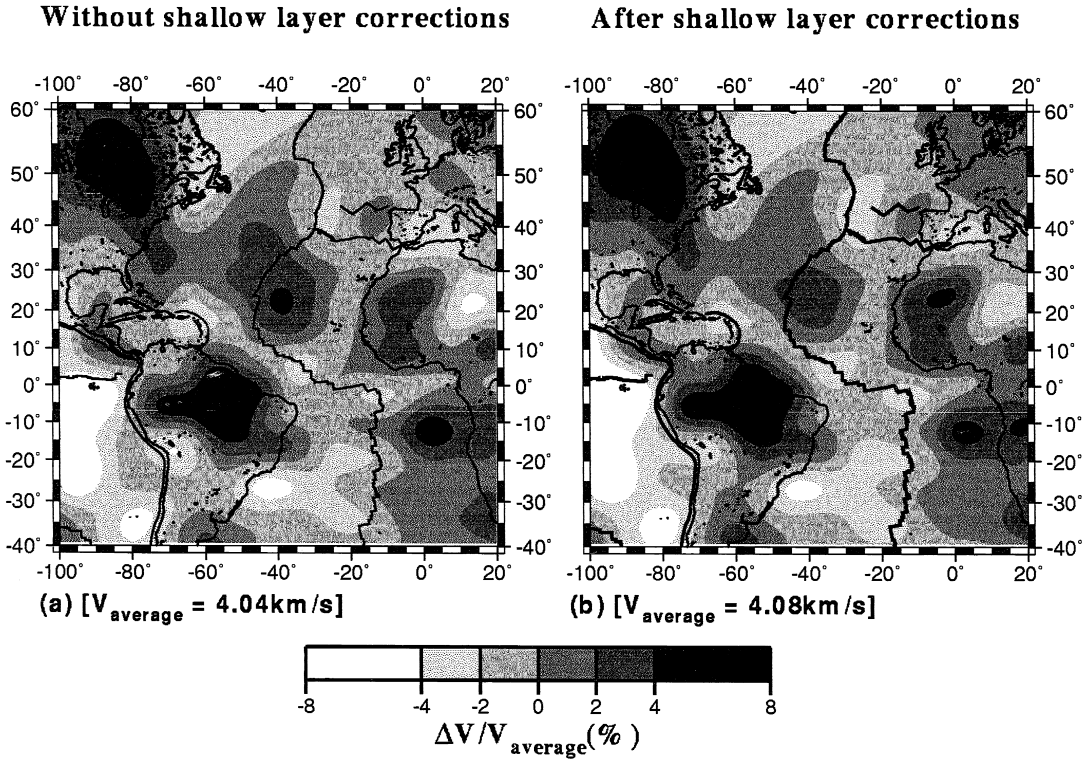

Fig. 8. Phase velocity perturbation maps obtained for a period of 62 s. The perturbations are computed with respect to the map average velocity $V_{average}$ and expressed in percent. (a) without shallow layers corrections [$V_{average} = 4.04$ km/s], (b) after shallow layer corrections [$V_{average} = 4.08$ km/s].

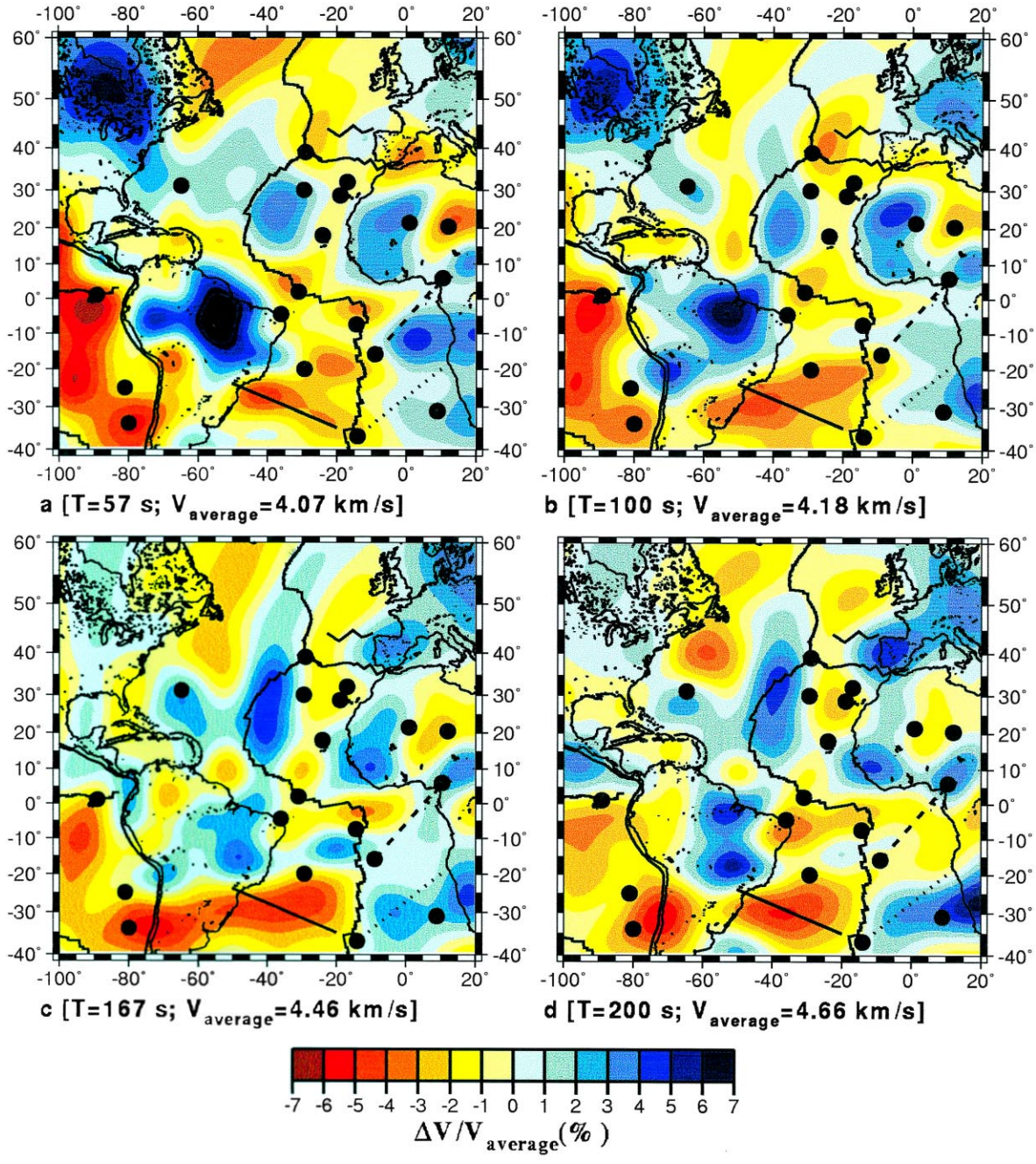

Fig. 9. Phase velocity perturbation maps obtained using the inversion parameters defined in Table 1. The perturbations are computed with respect to the map average velocity $V_{average}$ and expressed in percent. (a) $T = 57$ s, $V_{average} = 4.07$ km/s; (b) $T = 100$ s, $V_{average} = 4.18$ km/s; (c) $T = 167$ s $V_{average} = 4.46$ km/s; (d) $T = 200$ s; $V_{average} = 4.66$ km/s.

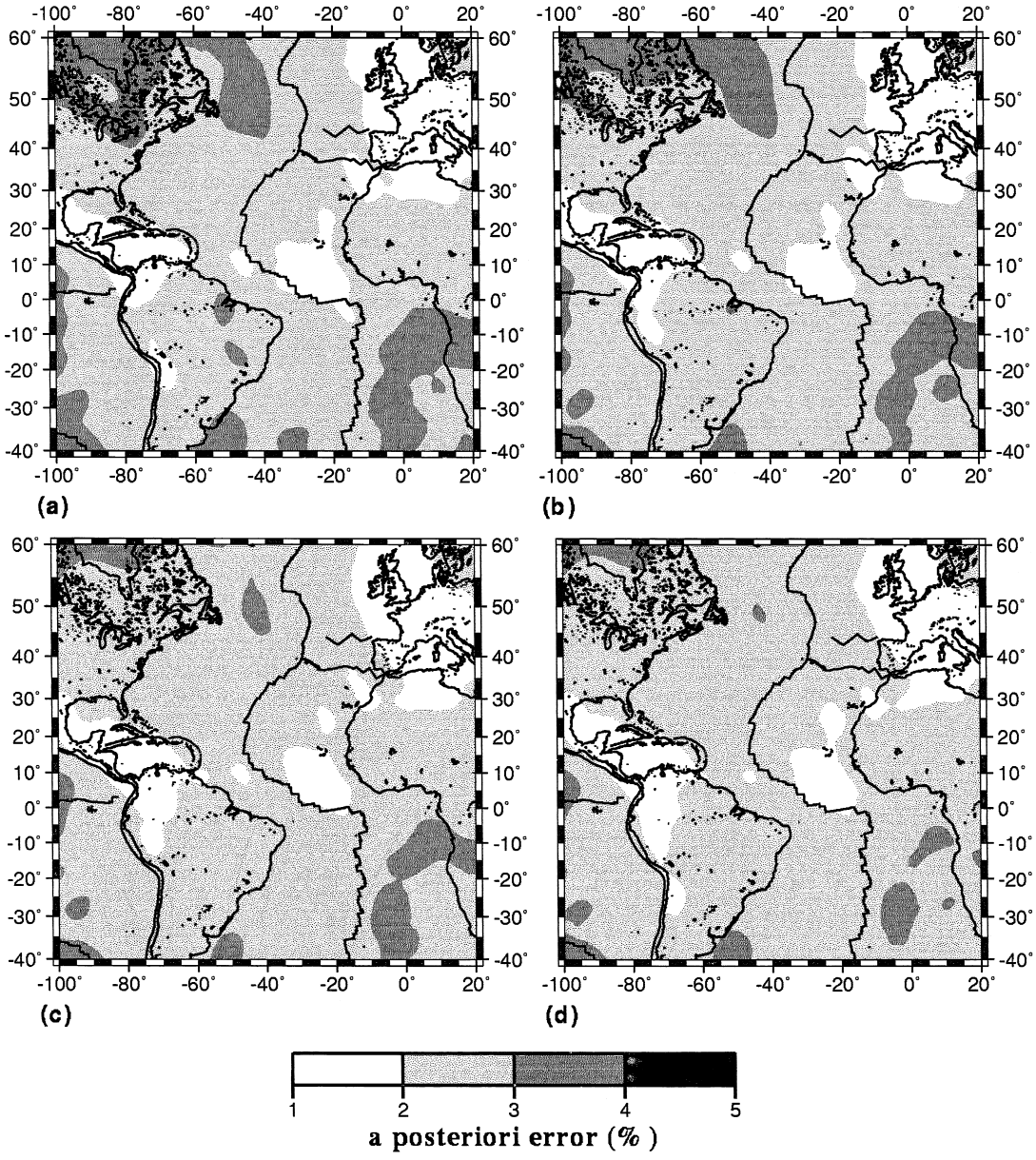

Fig. 10. A posteriori errors corresponding to the phase velocities presented in Fig. 9.

map displays a good correlation with the surface tectonics. For a comparison, Fig. 11 displays shields, ridges, hotspots and transform faults (Compilation from Crough, 1983; Melson and O'Hearn, 1986; Aslanian, 1993).

The MAR is the most visible feature of the Atlantic on global phase velocity maps (among others: Ekström et al., 1997; Trampert and Woodhouse, 1996; Zhang and Lay, 1996; Montagner and Tanimoto, 1990). It can clearly be associated with low

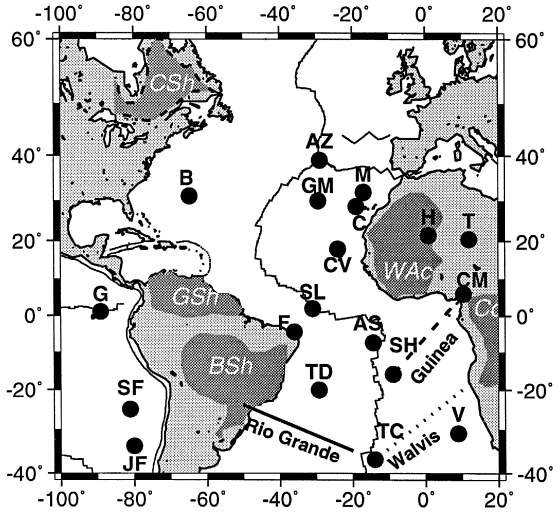

Fig. 11. Plate boundaries, hotspot locations and some geological features-after Crough (1983), Melson and O'Hearn (1986), Aslanian (1993). CSh, Canadian Shield; GSh, Guyana Shield; BSh, Brazilian Shield; WAc, West African craton; Cc, Congo craton. Circles designate hotspots, from top to bottom: AZ, Azores; M, Madeira; B, Bermuda; GM, Great Meteor; H, Hoggar; T, Tibesti; C, Canaries; CV, Cape Verde; CM, Cameroon; SL, Sierra Leone; (Schilling et al., 1994); G, Galapagos; F, Fernando de Noronha; AS, Ascension; SH, Santa Helena; TD, Trindade; SF, San Felix; V, Vema; TC, Tristan da Cunha; JF, Juan Fernandez. Lines correspond to hotspot traces.

velocities at short period (Fig. 9a). We can follow the MAR as well as the Rio Grande rise, and the Azores–Gibraltar fracture zone. When period increases (Fig. 9b,c,d), the MAR becomes less visible particularly in the North Atlantic, where the positive anomaly (already visible at 57 s) is shifted to the West to become centered on the ridge axis. This positive anomaly is also reported by Mocquet et al. (1989) and Van Heijst (personal communication, 1997) and confirms the shallow origin of the ridge. The Rio Grande rise is reported as a hotspot track, and the Azores–Gibraltar fracture zone both have a deeper origin because they still correspond to a low velocity anomaly for periods of 167 and 200 s (Fig. 9c–d).

We can separate the structure of South and North Atlantic: the North Atlantic displays higher velocities than the South Atlantic, meaning that it can be associated with colder structures than the South Atlantic. Moreover, for periods ranging from 50 to 170 s, the South Atlantic displays an asymmetrical structure with respect to the ridge, that is fast velocities at the East and slow velocities at the West of the ridge axis. This asymmetry is, however, not so visible in the North Atlantic.

A striking feature of the phase velocity maps is the good correlation between low velocities and hotspot surface locations (plotted with a dot in Fig. 9a–d) up to the largest period inverted (200 s, that correspond roughly to 300–400 km depth). A low velocity anomaly is coming out, elongated in a roughly North–South direction that follows the present hotspot surface locations. In South Atlantic, hotspots are located along the ridge axis, and the low velocity anomaly coincide with this ridge axis. In contrast, the low velocity anomaly in the North Atlantic is associated with hotspot locations and not with the ridge axis.

The shields in Brazil, Canada and Africa, as well as the oldest ocean basins in the North Atlantic correspond to high velocity anomalies at short period. When period increases, the Canadian shield high velocity anomaly decreases significantly, whereas Brazilian and African shields still correspond to a strong positive amplitude even at a period of 200 s. The positive anomaly beneath the Brazilian shield might be the trace at depth of the subducting plate.

Finally, the anomaly observed beneath the Eurasian–African boundary, between Iberia and North Africa, is no longer visible beyond 100 s showing that this is a shallow tectonic feature.

The results obtained by this regional study have been compared with the most recent global phase velocity maps obtained by Trampert and Woodhouse (1995, 1996), Ekström et al. (1997) and Zhang and Lay (1996). Fig. 12 presents, for a period of 100 s, the isotropics models of Trampert and Woodhouse (1996), Ekström et al. (1997) and our anisotropic model. The three models have similar correlation lengths and the anomalies are expressed in percent with respect to the PREM average velocity. The amplitude of anomalies is stronger in our study than in the global study because global models tend to filter out short wavelength features, whereas our regional maps maintain their presence. Although the principal features between the different models are

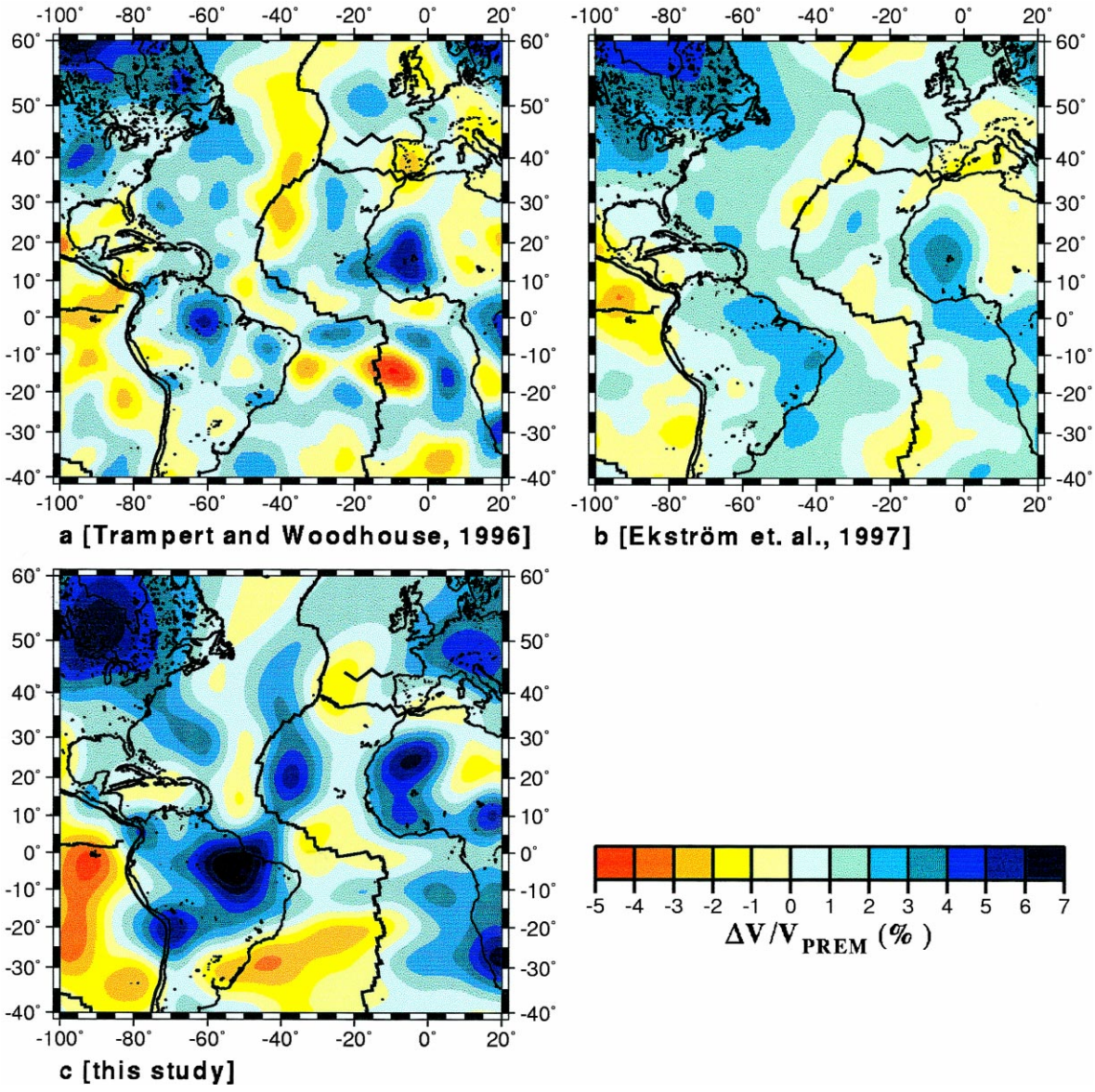

Fig. 12. Phase velocity perturbation maps for a period of 100 s. (a) Model of Trampert and Woodhouse (1996); (b) Model of Ekström et al. (1997); (c) our model; phase velocity variations are given in percent with respect to the PREM average velocity of 4.089 km/s.

consistent, the regional study gives a better resolution of small features. The main discrepancy between models concerns the asymmetry of the ridge in the South Atlantic (higher velocities at the East side than at the West side of the ridge). This asymmetry is observed in our model and is also reported by Zhang and Lay (1996). We observe the same feature at long period on the model from Trampert and Woodhouse (1995), but Ekström et al. (1997) display a symmetrical model with respect to the ridge.

4.2. Anisotropy directions

Data have been inverted for velocities and azimuthal anisotropy. An anisotropy pattern is presented in Fig. 13 for three periods: 57, 167 and

200 s. Anisotropy is plotted by a bar. The bar direction indicates Rayleigh wave fast direction, whereas, the bar length indicates the amplitude of the anisotropy.

The directions of the azimuthal fast axis of Rayleigh waves (Fig. 13) does not change much as a function of period, but the amplitude of anisotropy increases with increasing period. To resolve the anisotropy, it is necessary to have crossing paths coming from different azimuths. Because of the path distribution (Fig. 1), the well resolved area, in terms of anisotropy, is limited to Central Atlantic. In this area, we observe a good relationship between the Mid Atlantic ridge axis and anisotropy direction: the fast axis is perpendicular to the ridge and rotates when the ridge is curved. Under the Caribbean sea, we also observe a rotation of the fast direction which may reflect the direction of subduction. Finally, the

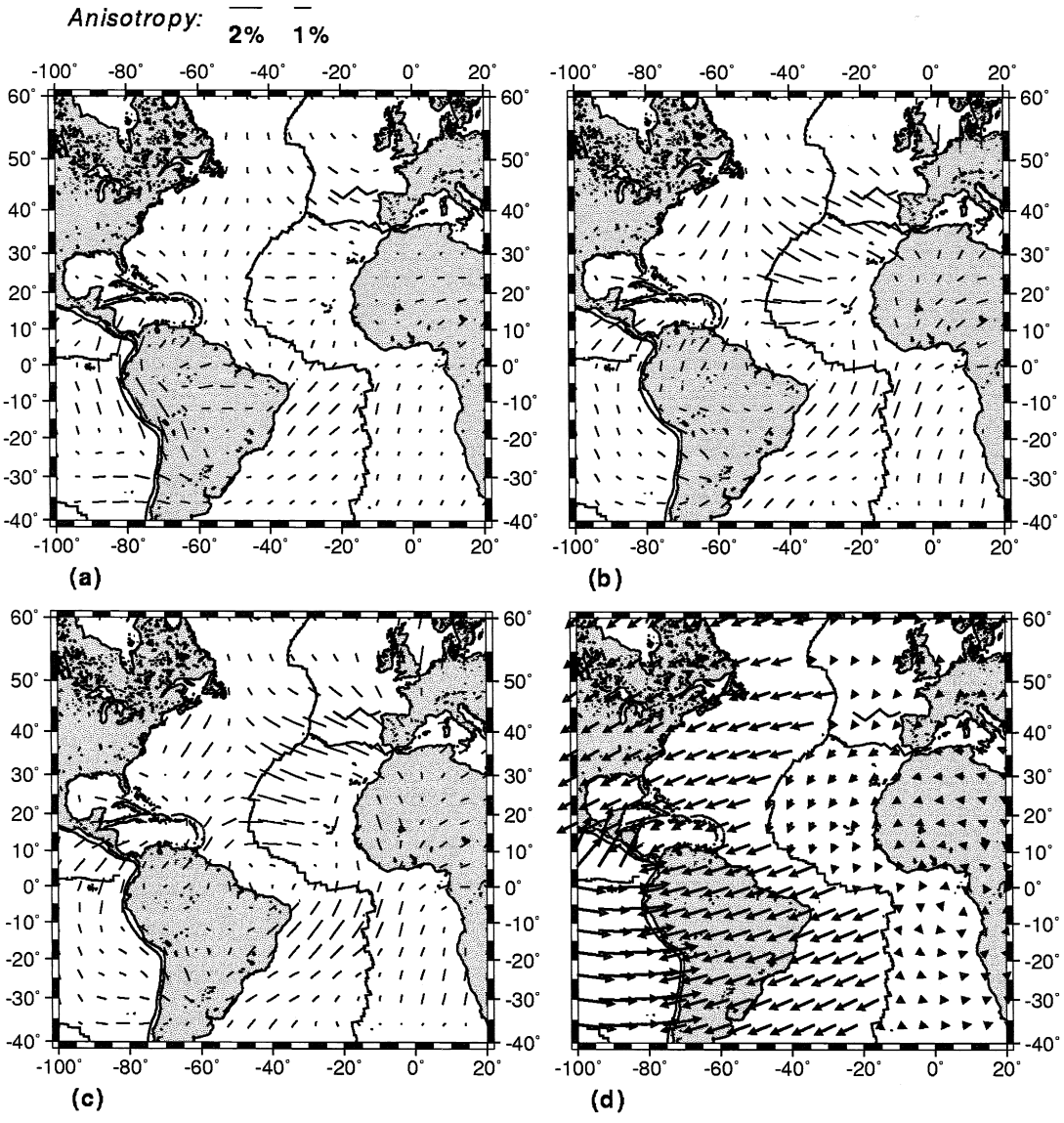

Fig. 13. Anisotropy Directions; (a) $T = 57$ s, (b) $T = 167$ s, (c) $T = 200$ s. A bar length of 5 mm corresponds to 2% of anisotropy.

western part of the North Atlantic shows a roughly North–South fast direction that is in agreement with the direction obtained by Kuo et al. (1987) from shear waves. Fig. 13d shows the current plate velocities relative to hotspots from Gripp and Gordon (1990). A comparison of seismic anisotropy directions with plate motion maps shows that anisotropy directions cannot be simply explained by plate motion. This means that seismic anisotropy probably integrates deeper phenomena, such as mantle convection.

5. Conclusions

The inversion of phase velocities obtained along 1311 paths crossing the Atlantic Ocean has enabled us to obtain a model of phase velocity and azimuthal anisotropy lateral variations. We have shown that anisotropy is necessary to explain the data. We have obtained maps with a lateral resolution of about 800 km. The phase velocity anomalies display stronger amplitudes than global tomographic models which filter out short wavelength features. Nevertheless, the location of anomalies is, in general, compatible with the different models. On average, the North Atlantic corresponds to higher velocities than the South Atlantic.

The ridge axis corresponds to a low velocity anomaly mainly visible at short period. A good correlation between hotspot locations and low velocity anomalies is obtained for the whole period range. Furthermore, a low velocity anomaly elongated along a North–South direction is visible for every period and seems to be correlated with hotspot positions.

The shields in Canada, Brazil and Africa correspond to high velocity anomalies at short period and only the Brazilian and African shields are still visible for a period of 200 s. This suggest that the Canadian shield is a shallow structure with a maximum depth extent of about 150–200 km, whereas the Brazilian and African shields roots are deeper than 300 km.

Anisotropy directions are only interpreted in the Mid-Atlantic area where they are best resolved. The fast axis of Rayleigh waves is found to be perpendicular to the ridge axis. It rotates when the ridge is curved. This anisotropy cannot be explained only by plate motions, and probably integrates deeper phenomena, such as mantle convection.

In order to better quantify the depth extent and characterisation of hotspots, a combined inversion of Rayleigh and Love wave phase velocity is now under progress.

Acknowledgements

The authors would like to thank A. Forte and G. Roult for helpful discussions, and B. Forte for reading this paper. The research presented here was performed using data from the GEOSCOPE and IRIS seismograph networks. This work has been supported by JNICT/CNRS Cooperation Program. This is IPGP contribution no. 1528.

References

Aslanian, D., 1993. Interactions entre les processus intraplaques et les processus d'accrétion océanique: l'apport du géoïde altimétrique. PhD Thesis. Brest.

Backus, G.E., 1970. A geometrical picture of anisotropic elastic tensors. Rev. Geophys. 8, 633–671.

Bussy, M., Montagner, J.P., Romanowicz, B., 1993. Tomographic study of upper mantle attenuation in the Pacific Ocean. Geophys. Res. Lett. 20, 663–666.

Canas, J.A., Mitchell, B.J., 1981. Rayleigh wave attenuation and its variation across the Atlantic Ocean. Geophys. J. R. Astron. Soc. 67, 159–176.

Crough, S.T., 1983. Hotspot swells. Annu. Rev. Earth Planet Sci. 11, 163–193.

Debayle, E., Lévêque, J.J., 1997. Upper mantle heterogeneities in the Indian Ocean from waveform inversion. Geophys. Res. Lett. 24, 245–248.

Dziewonski, A.M., Anderson, D.L., 1981. Preliminary reference Earth model. Phys. Earth Planet. Int. 25, 297–356.

Ekström, G., Tromp, J., Larson, E.W.F., 1997. Measurements and global models of surface waves propagation. J. Geophys. Res. 102, 8137–8157.

Forte, A., Woodward, R.L., Dziewonski, A.M., 1994. Joint inversions of seismic and geodynamic data for models of three-dimensional mantle heterogeneity. J. Geophys. Res. 99, 21857–21877.

Grand, S.P., 1994. Mantle shear structure beneath the Americas and surrounding. J. Geophys. Res. 99, 591–621.

Griot, D.A., 1997. Tomographie anisotrope de l'Asie Central à partir d'ondes de surface. Thèse de doctorat de l'Université de Paris VII.

Gripp, A.E., Gordon, R.G., 1990. Current plate velocities relative to the hotspots incorporating the NUVEL-1 global plate motion model. Geophys. Res. Lett. 17, 1109–1112.

Honda, S., Tanimoto, T., 1987. Regional 3-D heterogeneities by waveform inversion-application to the Atlantic area. Geophys. J. R. Astron. Soc. 94, 737–757.

Kuo, B.Y., Forsyth, D.W., 1992. A search for split SKS waveforms in the North Atlantic. Geophys. J. Int. 108, 557–574.

Kuo, B.Y., Forsyth, D.W., Wysession, M., 1987. Lateral heterogeneity and azimuthal anisotropy in the North Atlantic determined from SS–S differential travel times. J. Geophys. Res. 92, 6421–6436.

Li, X.D., Romanowicz, B., 1996. Global shear velocity model developed using non-linear asymptotic coupling theory. J. Geophys. Res. 101, 22245–22272.

Melson, W.G., O'Hearn, T., 1986. 'Zero-age' variations in the composition of abyssal volcanic rocks, The Geology of North America, Vol. M., The Western North Atlantic Region, The Geological Society of America, pp. 117–136.

Mocquet, A., Romanowicz, B., Montagner, J.P., 1989. Three-dimensional structure of the upper mantle beneath the Atlantic Ocean inferred from long-period Rayleigh waves: I. Group and phase velocity distributions. J. Geophys. Res. 94, 7449–7468.

Mocquet, A., Romanowicz, B., 1990. Three-dimensional structure of the upper mantle beneath the Atlantic Ocean inferred from long-period Rayleigh waves: II. Inversion. J. Geophys. Res. 95, 6787–6798.

Montagner, J.P., 1986a. Regional three-dimensional structures using long period surface waves. Ann. Geophys. 4 (B), 283–294.

Montagner, J.P., 1986b. First results on the three-dimensional structure of the Indian Ocean inferred from long-period surface waves. Geophys. Res. Lett. 13, 315–318.

Montagner, J.P., Jobert, N., 1988. Vectorial tomography: II. Application to the Indian Ocean. Geophys. J. 94, 309–344.

Montagner, J.P., Nataf, H.C., 1986. A simple method for inverting the azimuthal anisotropy of surface waves. J. Geophys. Res. 91, 511–520.

Montagner, J.P., Tanimoto, T., 1990. Global anisotropy in the upper mantle inferred from the regionalization of phase velocities. J. Geophys. Res. 95, 4797–4819.

Montagner, J.P., Tanimoto, T., 1991. Global upper mantle tomography of seismic velocities and anisotropies. J. Geophys. Res. 96, 20337–20351.

Nataf, H.-C., Ricard, Y., 1996. 3-SMAC: A tomografic model of the upper mantle based on a geophysical modelling. Phys. Earth Planet Int. 95, 101–122.

Schilling, J.G., Hanan, B.B., McCully, B., Kingsley, R.H., 1994. Influence of the Sierra Leone mantle plume on the equatorial Mid-Atlantic Ridge: a Nd–Sr–Pb isotopic study. J. Geophys. Res. 99, 12005–12028.

Sheehan, A.F., Solomon, S.C., 1991. Joint inversion of shear wave travel time residuals and geoid and depth anomalies for long-wavelength variations in upper mantle temperature and composition along the Mid-Atlantic Ridge. J. Geophys. Res. 96, 19981–20009.

Smith, M.L., Dahlen, F.A., 1973. The azimuthal dependence on Love and Rayleigh wave propagation in a slightly anisotropic medium. J. Geophys. Res. 78, 3321–3333.

Stutzmann, E., Montagner, J.P., 1994. Tomography of the transition zone from the inversion of higher-mode surface waves. Phys. Earth Planet. Int. 86, 99–116.

Tarantola, A., Valette, B., 1982. Generalized nonlinear inverse problems solved using least squares criterion. Rev. Geophys. Space Phys. 20, 219–232.

Trampert, J., Woodhouse, J.H., 1995. Global phase velocity maps of Love and Rayleigh waves between 40 and 150 seconds. Geophys. J. Int. 122, 675–690.

Trampert, J., Woodhouse, J.H., 1996. High resolution global phase velocity distributions. Geophys. Res. Lett. 25, 21–24.

Weidner, D.J., 1974. Rayleigh wave phase velocities in the Atlantic Ocean. Geophys. J. R. Astron. Soc. 36, 105–139.

Woodhouse, J.H., Girnius, T.P., 1982. Surface waves and free oscillations in a regionalized earth model. Geophys. J. R. Astron. Soc. 68, 653–673.

Yang, X., Fischer, K.M., 1994. Constraints on North Atlantic upper mantle anisotropy from S and SS phases. Geophys. Res. Lett. 21, 209–312.

Zhang, Y.S., Lay, T., 1996. Global surface wave phase velocity variations. J. Geophys. Res. 101, 8415–8436.